Biomicrofluidics ARTICLE scitation.org/journal/bmf

Low intermittent flow promotes rat mesenchymal stem cell differentiation in logarithmic fluid shear device

Cite as: Biomicrofluidics 14, 054107 (2020); doi: 10.1063/5.0024437
Submitted: 8 August 2020 · Accepted: 13 October 2020 ·
Published Online: 27 October 2020

Sanat Kumar Dash,[1] Vineeta Sharma,[2] Rama Shankar Verma,[2,a)] and Sarit K. Das[1,a)]

AFFILIATIONS

[1]Department of Mechanical Engineering, Indian Institute of Technology Madras, Chennai 600 036, India
[2]Department of Biotechnology, Indian Institute of Technology Madras, Chennai 600 036, India

[a)]**Authors to whom correspondence should be addressed:** vermars@iitm.ac.in and skdas@iitrpr.ac.in

ABSTRACT

Bone marrow mesenchymal stem cells are an ideal candidate for bone tissue engineering due to their osteogenic potential. Along with chemical, mechanical signals such as fluid shear stress have been found to influence their differentiation characteristics. But the range of fluid shear experienced *in vivo* is too wide and difficult to generate in a single device. We have designed a microfluidic device that could generate four orders of shear stresses on adherent cells. This was achieved using a unique hydraulic resistance combination and linear optimization to the lesser total length of the circuit, making the device compact and yet generating four logarithmically increasing shear stresses. Numerical simulation depicts that, at an inlet velocity of 160 μl/min, our device generated shear stresses from 1.03 Pa to 1.09 mPa. In this condition, we successfully cultured primary rat bone marrow mesenchymal stem cells (rBMSCs) in the device for a prolonged period of time in the incubator environment (four days). Higher cell proliferation rate was observed in the intermittent flow at 1.09 mPa. At 10 mPa, both upregulation of osteogenic genes and higher alkaline phosphatase activity were observed. These results suggest that the intermittent shear of the order of 10 mPa can competently enhance osteogenic differentiation of rBMSCs compared to static culture.

I. INTRODUCTION

Fluid shear stress (FSS) has been understood as an important cue in cellular mechanotransduction. Blood flows in the aorta to the interstitial flow inside tissues and everywhere cells are continually exposed to fluid shear. The magnitude of FSS in different tissues varies significantly and lead to generate tissue specific response. It has also been demonstrated that cells respond to FSS by changing their behavior in terms of proliferation, differentiation, alignment, cell shape, and cytoskeletal arrangement.[1,2]

Recent studies on mesenchymal stem cells (MSCs) have revealed the changes in differentiation and proliferation characteristics based on the FSS signal. FSS has been shown to control differentiation toward various lineages like osteogenic, chondrogenic, endothelial, myogenic, cardiomyogenic, neurogenic, etc.[3–5] It enhances osteogenic differentiation through increased activity of alkaline phosphatase (ALP), high collagen production, calcium deposition, upregulation of genes like osteopontin (OP) and oligosaccharyl transferase complex (OSTC), etc.[6] Osteogenic induction of MSCs varies with the frequency, magnitude, and duration of FSS.[7] For example, the rate of FSS has been found to be more effective in osteogenesis of MSCs than chemical stimulation and substrate stiffness stimulation.[8] Oscillatory shear stress (OSS) forms directional organization of human mesenchymal stem cells (hMSCs) and can lead to induction of morphological changes in them from spindle shape to round. It also induces increased expression of transcription factors like sex determining region box 2 (SOX2) and homebox protein nanog (NANOG), which are crucial in self-renewal of stem cells.[9] Induction of a proliferative response in hMSCs through extracellular signal-regulated kinase 1/2 (ERK1/2) and activation of calcium signaling through protein calcineurin are a few important consequences of OSS.[10] Slow and constant fluid flow has been shown to induce nuclear localization of tafazzin (TAZ) that is responsible for osteoblastic differentiation through genes like runt related transcription factor 2 (Runx2).[11] Low level fluid shear also promotes proliferation and differentiation of osteoblast progenitor cells, whereas greater FSS magnitude inhibited it.[12]

In fact, the intermittent fluid shear has been found to be more effective in osteogenesis than the continuous flow.[13]

Conventionally, different devices were used to study FSS mechanotransduction. Mostly, they are parallel plate flow chamber and cone and plate shear devices or a perfusion culture system in a porous matrix.[14–16] However, these devices can only produce a small range of stresses in selected experiments, and this creates difficulty in studying the wide range of physiologic shear stresses. The emergence of microfluidic technology has revolutionized the way biological studies have been done in the last decade. This technology allows ease of fabrication and greater control over the process to understand the physiological phenomenon in a microscale. Moreover, PDMS used in microfluidic device fabrication has good biocompatibility and oxygen permeability that assist to overcome the shortfalls of the previous designs used in the biological research. Delon *et al.* fabricated a shear device based on the Hele–Shaw stagnation flow that could generate varying shear (0–3 mPa) in a single channel.[17] Though single channel design is very convenient, it fails to do both on-chip and off-chip analyses. It also becomes difficult to pin point the boundary between the varying shear magnitudes. Such issues can be avoided by using parallel channels as culture chambers in the design. A microfluidic device with 10 parallel channels was developed by Chau *et al.*[18] This device produced shear stress from 0.07 to 13 Pa on the channel walls based on the difference in channel lengths. The main disadvantage of this device was that cells could not survive in the last channel because of very low nutrient flow rate. In another work reported by Booth *et al.*, generation of shear stresses from 0.1 to 6 Pa was done using eight parallel microfluidic chips.[19] These chips utilized a single peristaltic pump to study the effect of FSS on vascular endothelial cells. Here, they achieved the shear stress variation by changing both the channel length and the width. In a similar work, Kou *et al.* developed a device to study cytosolic calcium dynamics in osteoblasts triggered by FSS. It could produce a shear stress of 0.03 to 0.3 Pa in one run.[20] With the intention to keep same cell culture area for each shear values, a microfluidic perfusion system was fabricated by Zhong *et al.* Here, the device was comprised of defined cell culture chambers and resistance channels. They could generate a shear stress in the range of 0.7 mPa to 1.5 Pa by simultaneously running two devices at two different flow rates.[21]

None of the reported microfluidic devices were able to generate shear with the wide physiologic stress range on a single chip while keeping all other variables constant such as number cells in each culture chamber. In the present study, we have designed and simulated a microfluidic device that could produce shear stress of four different orders of magnitude in a single run. Hence, the wide range of stress experienced by cells *in vivo* (low shear stress in the interstitial level to the range of high shear stress experienced by cells in blood circulation) could be generated by the device.[19,22] Our device was designed following a unique hydraulic resistance optimization technique. Numerical simulations were performed in ANSYS Fluent to confirm the viability of the design. The depth of the chip was chosen in such a way that the cell aspect ratio (CAR = r/h; r being the cell height and h being the channel height) is far less than 0.5. This will enable the flow profile to vary negligibly when the cells are adhered onto the chamber surface than the naked device.[23] The effects of FSS on rat bone marrow stromal cells (rBMSCs) proliferation and differentiation were studied with this device at both intermittent and continuous flow style.

II. MATERIALS AND METHODS

A. Device design and computation

A hydraulic resistance model with an optimization technique was used for the design of the microfluidic device. This technique helped reduce the total channel length to a minimum. The device geometry was designed in Solidworks software (Dassault systemes, USA). Hexahedral dominant meshing of the geometry was done in ANSYS 16.1 (USA) workbench. Simulations were carried out in ANSYS Fluent for different inlet flow rates, and corresponding shear stresses were obtained for different cell culture chambers. Shear stress behavior for a channel depth of 100 μm was analyzed for different inlet flow rates.

Viscosity and density of basal media were measured by an Anton Paar automated microviscometer (Austria) and an Anton Paar density meter (Austria), respectively. The values obtained were used for simulation. Assumptions used in the Fluent model were Newtonian behavior of fluid and no-slip boundary condition at the wall. The pressures at all the outlets were kept atmospheric. The inlet flow velocity was kept uniform. Flow-induced deformation of the walls was also neglected for the model.

B. Device fabrication and experimental setup

The device was fabricated by the conventional photolithography method followed by the soft lithography technique.[24] The photomask was prepared based on the design in a local shop. All other photolithography procedures were done in the micro-electro-mechanical system (MEMS) lab, IIT Madras. Microchem SU-8 2075 negative photoresist was spin coated on a clean silicon wafer to the required thickness and exposed to UV light of 350 nm wavelength for cross-linking of resist. Prebake and post-bake steps were followed before and after cross-linking. Photoresist that was not cross-linked was washed away with a developer solution. This was followed by an isopropanol wash. The thickness of the resist was measured with the help of a Bruker contour elite X optical profilometer.

PDMS was procured from Dow Corning, and mold was prepared at a 10:1 ratio of PDMS to the curing agent. The mold was baked for 40 min at 80 °C. Inlet and outlet holes were punched into the mold after baking. A soda lime glass plate was cut into desired dimensions and dipped 1 h in concentrated sulfuric acid for cleaning. The cleaned glass plate and the PDMS mold were bonded with the help of a Diener oxygen plasma generator. Tubing and valves for the microfluidic setup were procured locally. A bubble trap was devised by closing the mouth of a 5 ml Eppendorf tube with a PDMS mold with holes for tubing.

C. Flow rate measurement

The flow rates through all chambers at different inlet flow rates were measured by collecting the fluid at each of the four outlets, and the result was compared with simulation. De-ionized (DI) water was used for all flow rate measurement experiments.

D. Microchannel surface modification and characterization

To improve collagen adsorption and form a better cell culture surface, microchannel walls were exposed to oxygen plasma and coated with 2% (3-aminopropyl) triethoxysilane (APTES) in ethanol for 10 min. After coating, channels were washed three times with 100% ethanol and dried by blowing air with a syringe. After drying, the device was baked at 120 °C for 90 min in an oven. This was followed by a wash with 70% isopropanol for sterilization and air drying inside a laminar hood. Finally, channels were coated overnight with 1.5 mg/ml rat tail collagen I (Sigma-Aldrich, USA) to promote cell attachment. The collagen coating density was maintained between 6 and 10 mg/cm^2 as per the manufacturer's protocol. After coating, the microfluidic device was preconditioned with a complete culture medium for another 6–8 h before seeding cells. Glass coverslips were modified with a similar procedure for static cell culture that here onward mentioned as SG. In order to study wettability and collagen adsorption on the modified surface, the contact angle of de-ionized water on coated glass coverslips was measured with a goniometer (Holmarc, India). Coated microfluidic devices were washed with Dulbecco's phosphate-buffered saline (DPBS) and fixed with 4% paraformaldehyde (PFA) to prepare for collagen antibody staining. Next, they were incubated with a blocking buffer (1% BSA in PBST) for 30 min to avoid unspecific binding of anti-collagen antibodies. Overnight staining of collagen coating was undertaken with anti-collagen I primary antibody (Cell Signalling Technology, USA) at 4 °C followed by incubation with a secondary antibody (Thermo-Fisher Scientific, USA) for 1 h at room temperature. Bright-field and fluorescent images were taken using a fluorescent microscope (Nikon Eclipse Ti, Japan).

E. Cell isolation and culture

rBMSCs were isolated and cultured using the modified protocol of Soleimani and Nadri as done in our previous works.[25–28] In brief, Wistar rats of about 6–8 week old (~100 g) were sacrificed by cervical dislocation. The rats were dissected, and femur and tibia were removed. The bone marrow was aspirated using 22 gauge needle, and cells were collected in 10 ml of the basal medium containing alpha-MEM (Invitrogen, USA) supplemented with 10% FBS, 100 U/ml penicillin, and 100 mg/ml streptomycin. The aspirated bone marrow was washed twice using DPBSA at 150 g and re-suspended in alpha-MEM. The cells were then plated in a tissue culture flask and incubated at 37 °C in a humidified atmosphere containing 5% CO_2. After 8 h, the supernatant containing non-adherent cells was discarded, and the culture medium was replaced. Replacement of the culture medium was done every 8 h till 72 h of initial seeding. Further replacement of the culture medium was performed every third day till the cells attained about 90% confluence. Near confluence cells were passaged using 0.25% trypsin for 2 min at room temperature. Purity of cell population was studied with fluorescence-activated cell sorting (FACS). Basal media were added with osteogenic differentiation supplements, namely, dexamethasone (100 nM), ascorbic acid (50 μg/ml), and beta-glycerophosphate (10 mM), for all experiments.

F. Cell seeding in the microfluidic device

All experiments were performed with rBMSCs between third and sixth passage only. Cells were counted using a hemocytometer and seeded approximately at a density of 2–3 million cells/ml in order to attain near confluence. The device was incubated at 37 °C in a humidified atmosphere containing 5% CO_2 along with the syringe pump and tubing. Media circulation was started after cell attachment with osteogenic differentiation supplements. Similarly, cells were seeded on modified glass coverslips (SG) as static culture. Media were changed every 2 days during all experiments. Cell images were taken using a fluorescent microscope (Nikon Eclipse Ti) and compared for different shear rates.

G. Cell morphology and proliferation analysis

Cells for experiments were counted using the hemocytometer, and the same cell suspension was used for seeding all experimental groups. For static culture, the initial seeding density was taken from hemocytometer reading. For the microfluidic device, just after seeding, bright-field images were taken and the cell number was calculated manually in each image. The total cell number in a chamber was calculated by extrapolating the mean cell number from five different foci to the total area of the culture chamber. This was performed so as to neglect the spillage of a few cells to the outlet hole in the device due to inertia. After the shear experiments, cells were fixed with 4% PFA and stained with the Hoechst dye followed by wash with DPBS (2×). Images were taken using a fluorescent microscope, and cell numbers were calculated based on the number of fluorescence spots of fixed cells and extrapolated as before. Cell proliferation was calculated comparing this cell count with the initial number of cells seeded. It was assumed that the cell attachment efficiency was 100%, and there was negligible loss in cell during the staining procedure. Image processing was done with the help of ImageJ software.

H. Real time-polymerase chain reaction

Cells were extracted from each chamber through trypsinization, and the total RNA was converted to cDNA using cells to cDNA II kit (Thermofisher, USA) as per the manufacturer's protocol. SYBR Green I master mix (Takara, Japan) was used to detect real time-polymerase chain reaction (qRT-PCR) products. The products were amplified for 40 cycles using the default protocol. Primers for all the genes were designed with the help of NCBI-Primer blast. ΔCt value was calculated taking 100% pcr efficiency for both target and reference genes, and fold change was plotted.

I. Alkaline phosphatase assay

ALP activity was estimated through decomposition of *p*-nitrophenyl phosphate (*p*-NPP) to *p*-nitrophenol by the enzyme. Trypsinized cells were washed twice with DPBS, and each sample was re-suspended in 25 μl. 10 μl of cell suspension was incubated in 100 μl of Hoechst solution. Another 10 μl was incubated in 100 μl of 10 mM *p*-NPP in the assay buffer (100 mM Tris-HCl, 100 mM NaCl, 5 mM MgCl2). After 1 h incubation at room temperature, the reaction was stopped by adding equal volume of stop solution

(10 mM EDTA, 20 mM Tris-HCl). Absorbance of the reaction products at 405 nm was obtained by a micro-plate reader (EnVision, Perkin-Elmer, USA). Normalization of absorbance reading with cell number was undertaken by measuring Hoechst fluorescence for each sample.

J. Statistical analysis

The data were analyzed using two-way ANOVA using Graph Pad Prism5. Results were expressed as means ± SEM, and the values where $P < 0.05$ were taken as statistically significant.

K. Ethics approval

Ethics approval has been obtained for all animal experiments as per IIT Madras committee for the purpose of control and supervision of experiments on animals (ID No.: 1007/C/06/CPCSEA/IITM/BT/10/RSV-2018).

III. RESULTS

A. Design of the device

We used the hydraulic resistance model for microfluidic low Reynolds number flows to generate the hydraulic circuit. Previously, other groups used only parallel channels to obtain a range of shear stresses as shown in Fig. 1(a). In such a design, the flow rates in the culture chambers (R_c) can be changed by changing the resistances R_1, R_2, and R_3. However, these designs may fail to generate a compact device when shear stress varies by four orders of magnitude or more between the channels. Reduction of flow rate in a channel by such a high magnitude needs a similar increase in corresponding fluidic resistance value. This will increase the length of the channels and make the device bulky and prone to clogging. To improvise this, we have used a novel combination of series and parallel resistances.[29] It starts with a basic resistance circuit having only four resistors as shown in Fig. 1(b). Now, as per the requirement, the flow rates through resistances R_1, R_2, and R_3 have to be logarithmic. This was achieved by modulating all four resistance values with a linear

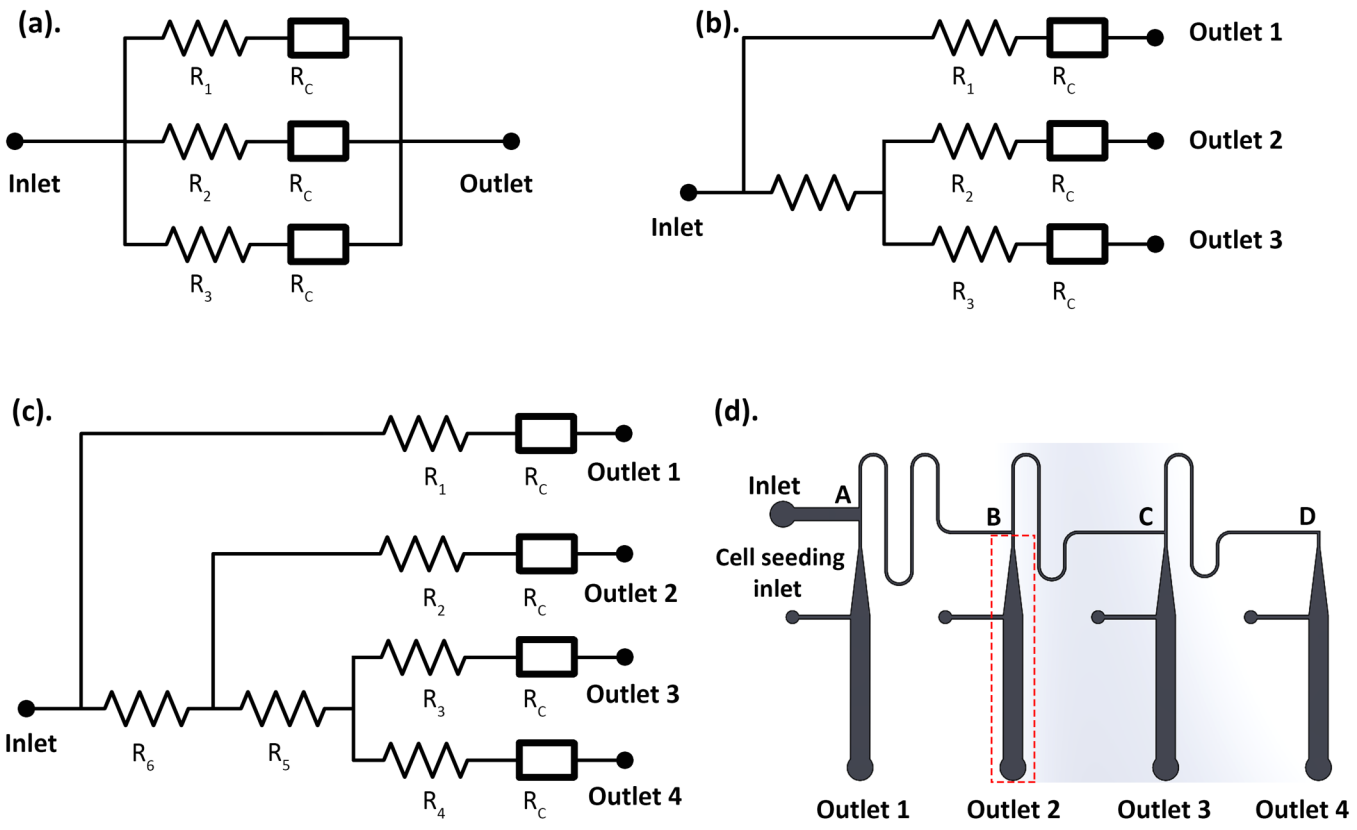

FIG. 1. (a) Conventional parallel channel arrangement with culture chambers denoted by resistance R_c. Different flow rates in the channels can be generated leading to various shear stress by altering the resistances R_1 to R_3. (b) Basic resistance model showing series and parallel combination of resistances for the optimized device. Flow rate decreases logarithmically from outlet 1 to 3. (c). Final circuit for a four chamber device. Flow rate is decreasing logarithmically from chamber 1 to 4. (d) Top view of the solidworks model of the device. Resistances corresponding to R_6, R_5, and R_4 are the channels from point A to B, from B to C, and from C to D, respectively. Region enclosed by a red dashed square is a culture chamber with resistance R_c.

optimization function leading to a minimized total resistance. The optimization function and the constraints for the basic circuit are

$$\text{Minimize: } R = R_1 + R_2 + R_3 + R_4 + 3R_c. \tag{1}$$

With constraints,

$$10Q_3 = Q_2 \text{ or } (R_3 + R_c) = 10(R_2 + R_c), \tag{2}$$

$$10Q_4 = Q_1, \tag{3}$$

$$R_1, R_2, R_3, R_4 \geq 0, \tag{4}$$

where R_i is the resistance of a channel and Q_i is the corresponding flow rate in that channel (i = 1, 2, 3, and 4). R_c is the resistance of the cell culture chamber. Constraint equations (2) and (3) are formulated in order to have the desired logarithmic flow rate. Based on the constraint equation (3), R_1 wing is the fastest channel in the design. Hence, it will have the lowest resistance possible or

$$R_1 = 0. \tag{5}$$

Using the relations from Eqs. (2) to (5) and rewriting the optimization function in terms of R_2, the total resistance becomes

$$R = 11R_2 + 22R_c - \frac{10(R_2 + R_c)}{11}. \tag{6}$$

Now, this value will be minimum when R_2 will be minimum; i.e., $R_2 = 0$.

Hence, the values of resistances are

$$R_3 = 9R_c, \tag{7}$$

$$R_1 = R_2 = 0, \tag{8}$$

$$R_4 = \frac{100}{11}R_c. \tag{9}$$

Constraint $10Q_3 = Q_2$ was taken instead of $Q_3 = 10Q_2$ as the minimum total resistance R will become larger in the latter case when the design is extended (calculation not shown). This basic design was extended to incorporate four resistance wings [Fig. 1(c)]. Each wing will contain a cell culture chamber to have the logarithmic flow distributions. The cell culture chambers were placed in wings having resistances R_1, R_2, R_3, and R_4. The values of resistances were found to be

$$R_1 = R_2 = R_3 = 0, \tag{10}$$

$$R_4 = 9R_c, \tag{11}$$

$$R_5 = R_6 = \frac{100}{11}R_c. \tag{12}$$

For further numerical calculations, approximate hydraulic resistance for the rectangular cross section channel was taken as

$$R = \frac{12\mu l}{1 - 0.63\left(\frac{h}{w}\right)} \times \frac{1}{h^3 w}, \tag{13}$$

where R is the hydraulic resistance of channel; μ is the coefficient of dynamic viscosity; and h, w, and l are height, width, and length of the microfluidic channel, respectively.[30] For a variable cross section channel, the resistance value was calculated by integrating this resistance value over the length.

All four culture chambers were designed to be of same dimensions. This helped to keep same sample volume for all shear stress conditions. The culture chamber consists of a diverging section and a rectangular section following it. The angle of the diverging part was kept at 7° to avoid separation of the fluid from the wall. Rectangular part, where cells were seeded, is kept 10 mm in length and 1.5 mm width to ensure a constant shear stress profile and a decent volume of sample. All intersections of channels were made T-type to avoid maldistribution of fluid in the daughter channels due to geometrical constraints. All other channels except the culture chamber were 200 μm wide. The seeding inlet was placed just after the diverging part in the culture chamber. With the device inlet closed, seeding collagen or cells through this resulted in minimal leakage to resistance channels, as the fluid preferred the low resistance path. The final solidworks model of the device is shown in Fig. 1(d). It shows the position of cell culture chambers and resistance channels along with cell seeding inlets. The experimental setup consists of a syringe pump, two one-way valves, the microfluidic device, a bubble trap, and a collection tank (Fig. 2).

B. Computational simulation

The present study proposes a microfluidic device that produces FSS of four different orders of magnitude in a single run for mechanotransduction studies of cells. Shear stresses on the cells were assumed to be of the same value as experienced by the chamber walls based on the negligible height of adhered cells and the CAR value. To estimate the shear stresses on culture chamber walls, the flow in the device was simulated using the Poiseuille flow model. The viscosity of basal media at 37 °C incubator temperature was measured to be 1.04 ± 0.04 mPa s. Density was found to be the same as water (1000 kg/m^3). These values were used for all simulations. FSS in the bottom wall of each chamber was extracted from ANSYS Fluent after fluid flow simulations. The value of shear stress was found to be decreasing logarithmically in simulations as predicted during device design for flow rates ranging from 0.1 to 1 ml/min. They were also found to be varying linearly with the inlet flow rate in each chamber. Figure 3(a) shows the logarithmic distribution at the inlet flow rate of 1 ml/min. Shear stress at 1 ml/min on a central line in the first culture chamber was estimated (6.23 Pa) as shown in Fig. 3(b). We can see that the value is constant shortly after the diverging portion of the chamber. Even at this high stress value, the profile was almost uniform in the transverse direction. This leads to the assumption that around 90% of cells would be experiencing similar shear magnitude. For

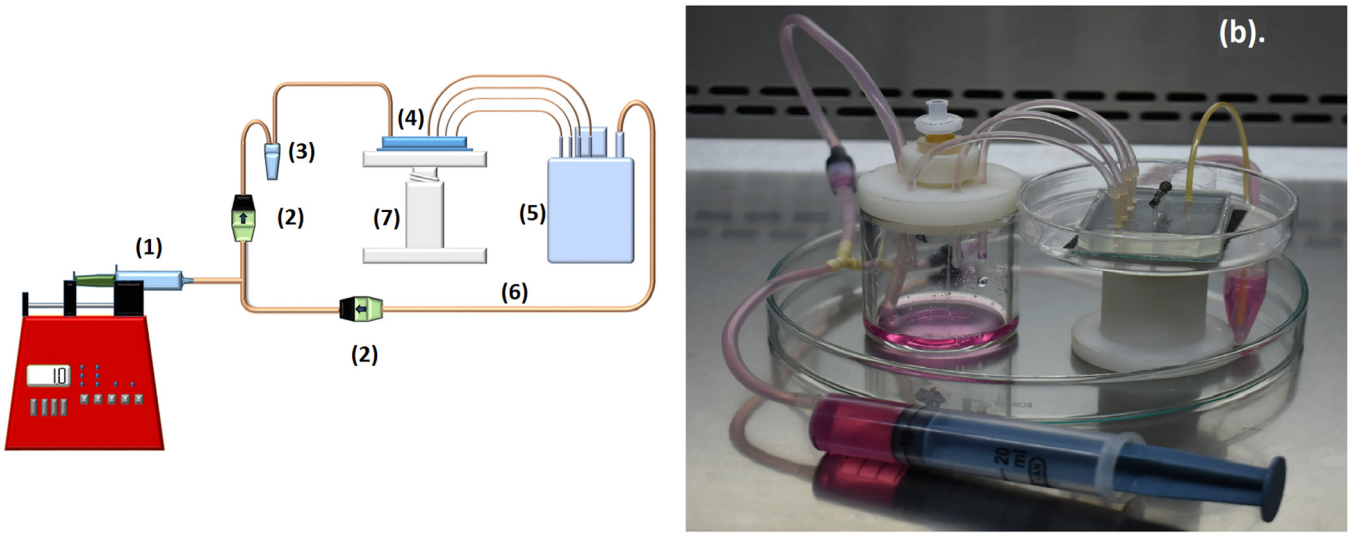

FIG. 2. (a) Experimental setup for shear flow assay. (1) Syringe pump. (2) Check valve. (3) Bubble trap. (4) Microfluidic device. (5) Media collection tank. (6) Tubings. (7) Movable stand for the device. All the equipments were kept inside the CO_2 incubator. The height of the outlet tubes from the table top was measured, and based on that, the stand height was selected. The stand has a screw thread arrangement that can increase or decrease its height. On the top of the media sink, a 0.22 μm filter was placed for air exchange. (b) Microfluidic setup inside the laminar flow hood.

mechanotransduction experiments, a maximum shear stress of 1 Pa was taken, and correspondingly, the inlet flow rate was set at 160 μl/min. This was based on the linear relationship of shear and inlet flow rate found in simulations (Fig. S7 in the supplementary material). Shear stresses at this inlet flow rates were 1.03 Pa, 101.9 mPa, 10 mPa, and 1.09 mPa from chamber 1 through 4, respectively, which cover shear stress range experienced *in vivo*[31] (Fig. 4).

To compute the effect of outlet tubing on the flow distribution in the chambers, simulations were carried out taking outlet pipe ID as 1.5 mm. Without gravity, the extended outlet up to 300 mm had a negligible effect in flow distribution as the hydraulic resistance value was very less compared to that of the channels in the device. In order to estimate the flow-induced deformation of the PDMS wall, flow rate variation as formulated by Gervais *et al.*[32] was

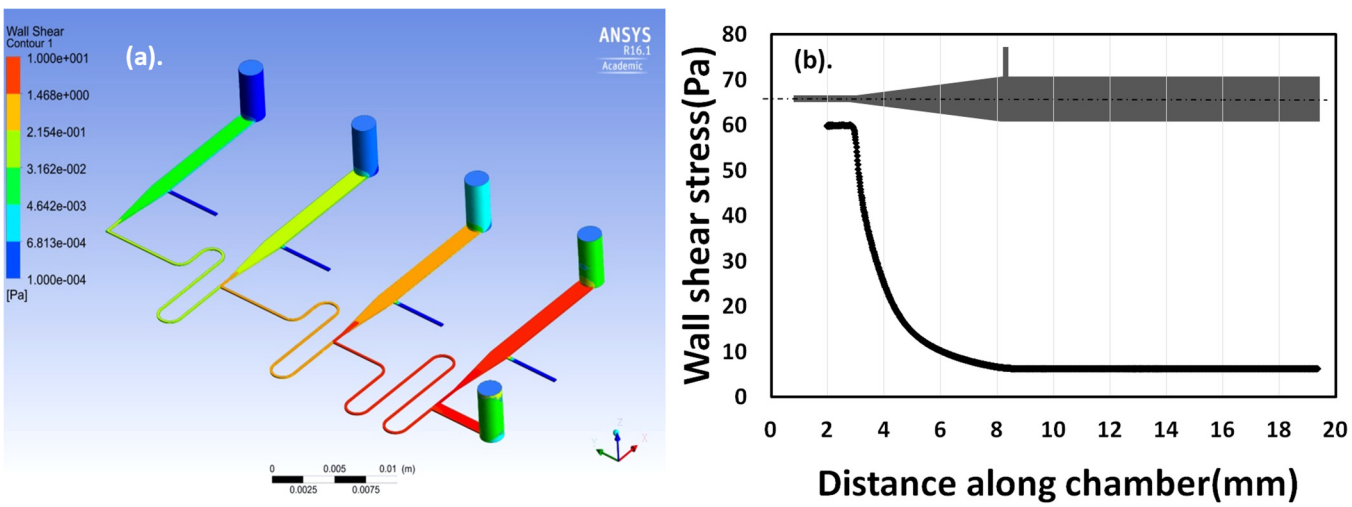

FIG. 3. (a) CFD post-processing contour showing shear stress distribution on the device chamber walls at 1 ml/min. Proper logarithmic distribution of stress in the chambers could be seen. (b) Shear stress development on the bottom wall along the mid-line in the first chamber at 1 ml/min inlet flow rate. It shows that the stress value becomes constant everywhere in the rectangular portion of the culture chamber where cells are seeded.

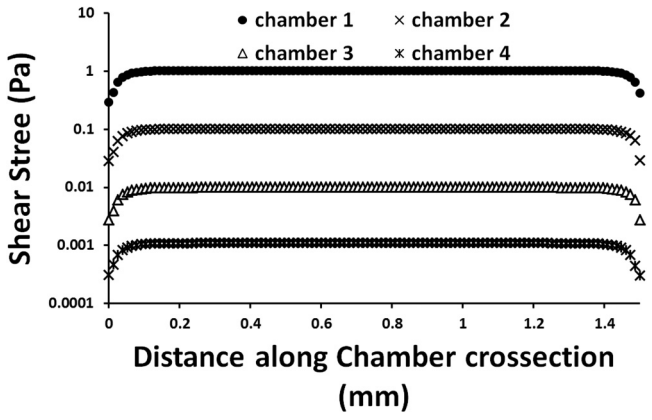

FIG. 4. Shear stresses on different chambers at an inlet flow rate of 160 μl/min on the bottom wall where cells are adhered. Shear value is mostly constant along the width of the channel which allows cells to experience a similar value of FSS almost everywhere in a chamber.

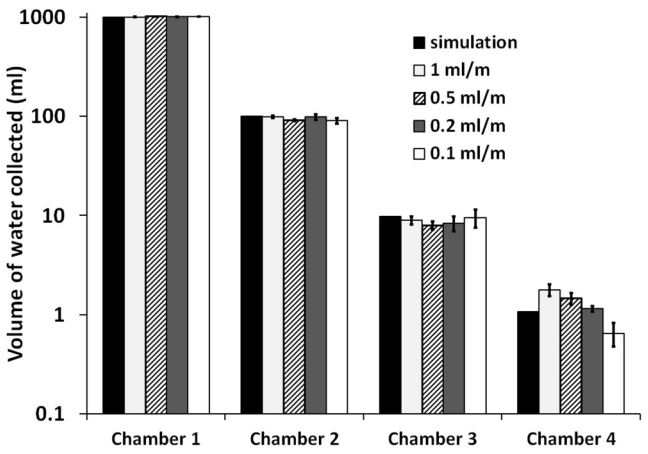

FIG. 5. Normalized simulation vs experimental volume collected at different inlet flow rates in different chamber outlets.

calculated taking Young's modulus from Johnston *et al.*[33] The formula is given as

$$\frac{\Delta Q}{Q} = \frac{Q_{deform} - Q_{rigid}}{Q_{rigid}} \approx \frac{3\alpha}{2}\frac{\Delta pW}{Eh_0}. \quad (14)$$

Taking $\alpha = 1$, which is the maximum value, $\Delta Q/Q$ came out to be of the order of 0.05 that is very small. Hence, deformation was neglected in further calculations.

C. Flow rate validation experiments

The fluid shear device was fabricated by the SU8 photolithography method. The spinning process was optimized to get a thickness close to 100 μm. The final thickness of the resist on the silicon master was found to be 101.6 ± 3 μm as measured by the optical profilometer. After fabrication of the PDMS device, it was tested for the flow rate distribution in each culture chamber. For different inlet flow rates, de-ionized (DI) water was collected at each outlet. The collected volumes were measured and normalized to 1111 ml of water supplied through the inlet. Results obtained were very much similar to the simulation results for different flow rates (Fig. 5). Similar flow distribution was also observed when media were perfused inside the incubator environment (Videos 1 and 2 in the supplementary material).

The pressure drop in the fourth chamber was in the order of few Pa (1–6 Pa). Hence, computation and experiments were carried out to check whether the addition of gravity affects the flow rate distribution in the channels. Experiments were conducted up to an outlet position of 40 mm below the device level. Both simulation and experiments showed no change in results when the outlets were kept at the same level from the device plane (data not shown).

D. Device coating and characterization

Glass surface has generally zero net charge. Due to this reason, cell attachment on glass is less efficient than tissue culture plastics as the latter are mostly negatively charged to promote cell attachment. Coating with an extracellular matrix (ECM) protein on glass is generally done to improve its ability to promote cell attachment. But the stability of the coating is a prime issue. For this reason, we precoated the glass surface with (3-aminopropyl) triethoxysilane (APTES), which can enhance collagen adsorption and provide a better cell attachment surface.[34,35] The surface with silane + collagen coating was found to have a lesser water contact angle than the collagen coated glass surface without silane (Fig. 6). To further confirm the suitability of the coated glass surface, it was stained with an anti-collagen antibody, and fluorescence was compared between silane + collagen and only collagen surfaces. Relative fluorescence of silane + collagen surface was found to be 1.34 ± 0.11 times more than only collagen coating as quantified through ImageJ software.

E. Flow and cell proliferation

Cells isolated from rats were spindle in shape and showed the characteristic morphology of MSCs. Flow analysis elucidated that $66.97 \pm 1.76\%$ cells were expressing CD29, $84.53 \pm 0.55\%$ cells were expressing CD 90, and only $14.10 \pm 2.17\%$ cells were expressing CD45 (Fig. S2 in the supplementary material). CD29 and CD90 were positive markers, and CD45 was the negative marker for MSC characterization.[36]

The flow experiments were divided into two time points, 1 day and 4 days, with two types of flow profile, continuous and intermittent for each time point.[13] A constant flow rate of 160 μl/min was set to get a continuous flow profile. For intermittent flow system, the syringe pump was programmed to deliver media at the same flow rate in a cyclic manner with 1 h run followed by 7 h stop. This 1:7 flow cycle was adopted to get proper media replenishment for cell survival in the slowest chamber (4th) with

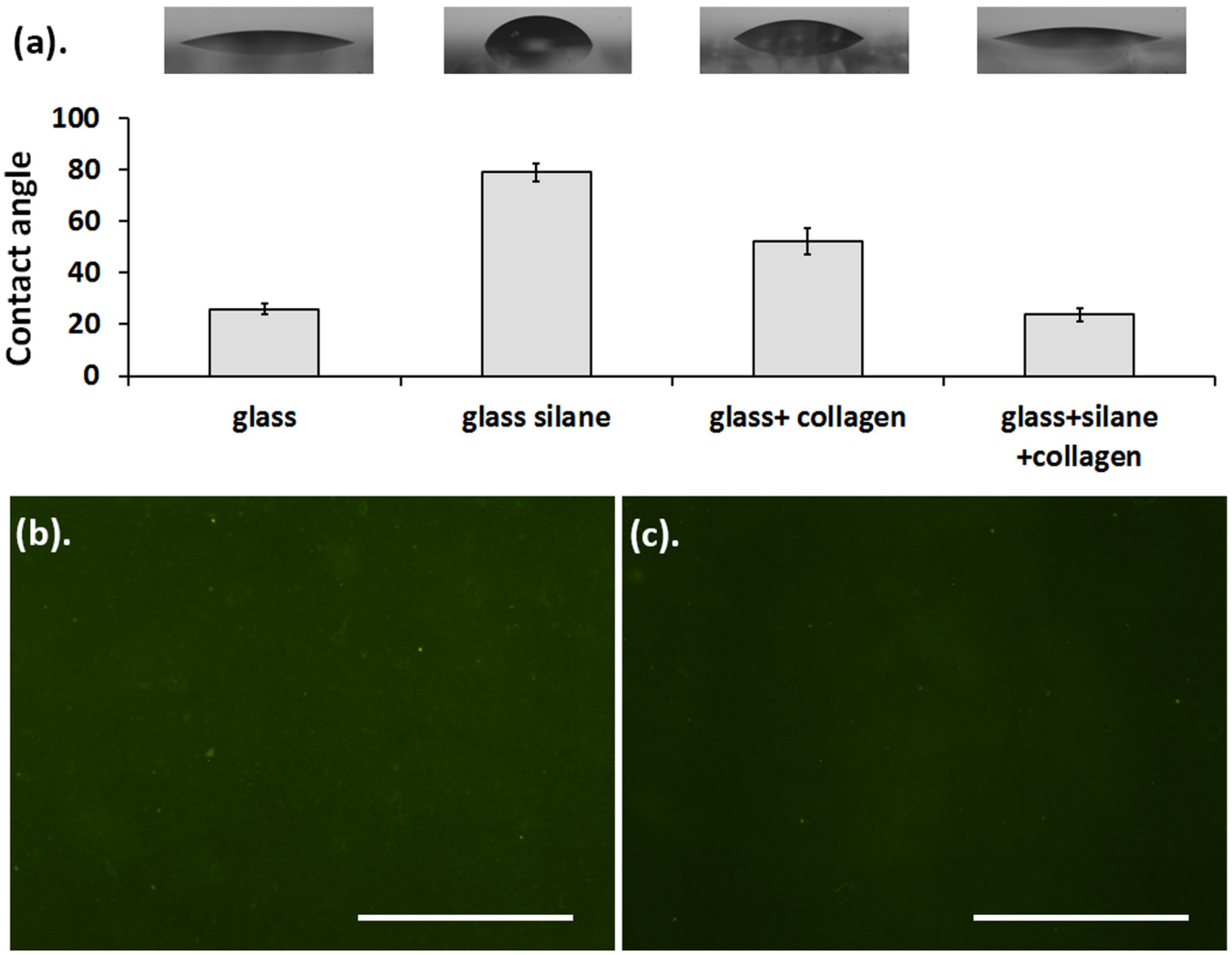

FIG. 6. (a) Contact angle measurement with different coating on the glass surface. The respective contact angles in degrees are 26, 79, 52, and 24. (b) Collagen antibody staining of glass surfaces after coating on the glass surface coated with silane and collagen. (c) Antibody staining of the glass surface coated with only collagen. Scale bar = 100 μm.

maximum possible dwell in between flow phases. Henceforth, the experimental groups are named as CC1 to CC4 for continuous flow group chamber 1 to 4 and IC1 to IC4 for intermittent flow group chamber 1 to 4.

Flow was started after 40 h of seeding so as to give cells enough time for proper adherence. During this time, every 8 h media were replaced in the device. After 1 day of flow, we did not observe any change in morphology for any experimental group (Fig. S3 in the supplementary material). But after 4 days of flow, cells in CC1 seemed to round up or detach (Fig. 7). Such behavior was witnessed in CC2 and CC3 as well but with lesser effect. Cell morphology at day 2 illustrated noticeable detachment from CC1. CC2 and CC3 showed this behavior on subsequent days (days 3 and 4, respectively, Fig. S4 in the supplementary material). The FSS in CC3 is moderate (10 mPa) but still detachment was observed, which raised concern of paracrine signaling from CC1 and CC2. In order to neglect such signaling, we run the device at 100 times less flow rate seeding cells only in CC1 to mimic CC3 with the original flow rate. Similar detachment of cells still occurred with this configuration. These data showed that continuous high magnitude shear ($\geq$10 mPa) could be detrimental to rBMSCs. In CC4, which has 10 times less shear than CC3, cells seemed to be healthy, adhered, and proliferating after 4 days. None of the intermittent flow chambers showed similar cell detachment.

Proliferation data at day 1 indicate a decrease in cell count in CC1 with very high statistical significance (Fig. 8). This indicates

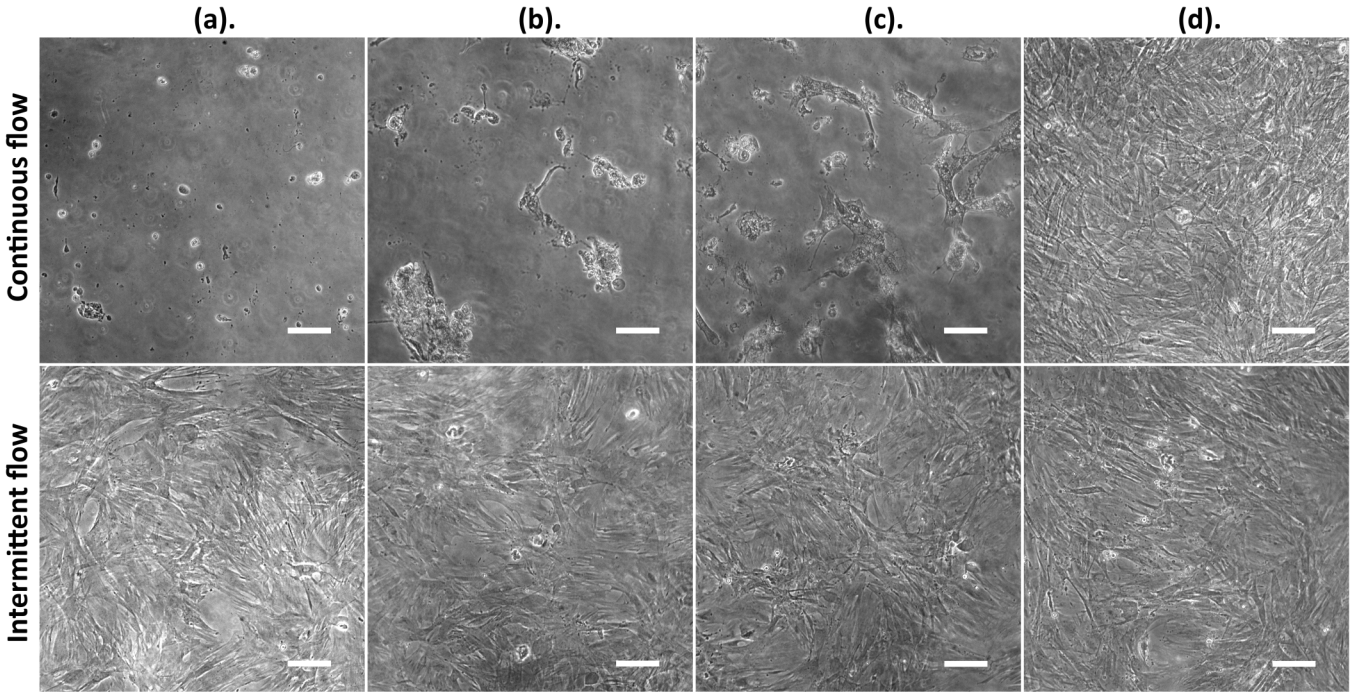

FIG. 7. Cell morphology after 4 days of flow. Top panel: continuous flow; bottom panel: intermittent flow. Column (a)–(d), chamber 1 through 4, respectively. Flow from bottom to top. Scale bar = 100 μm.

the onset of cell detachment, though morphologically the cells in all chambers look similar. Cell proliferation was observed for other chambers in the continuous flow group (CC2, CC3, and CC4) after 1 day. However, in CC2, the difference in the proliferation rate was significantly less than the control, whereas in CC4, it was significantly high. For the intermittent flow group, the proliferation was not significant except for IC4. After 4 days of flow, the proliferation rate was highest in IC4 with very high statistical significance, which provided the least stress. These data were in agreement with an earlier report.[37] In contrast, in all other chambers after 4 days of flow, cell proliferation was lesser than the static control group. As cells seem to detach from the first three chambers in the continuous experimental group, their proliferation rates were not calculated.

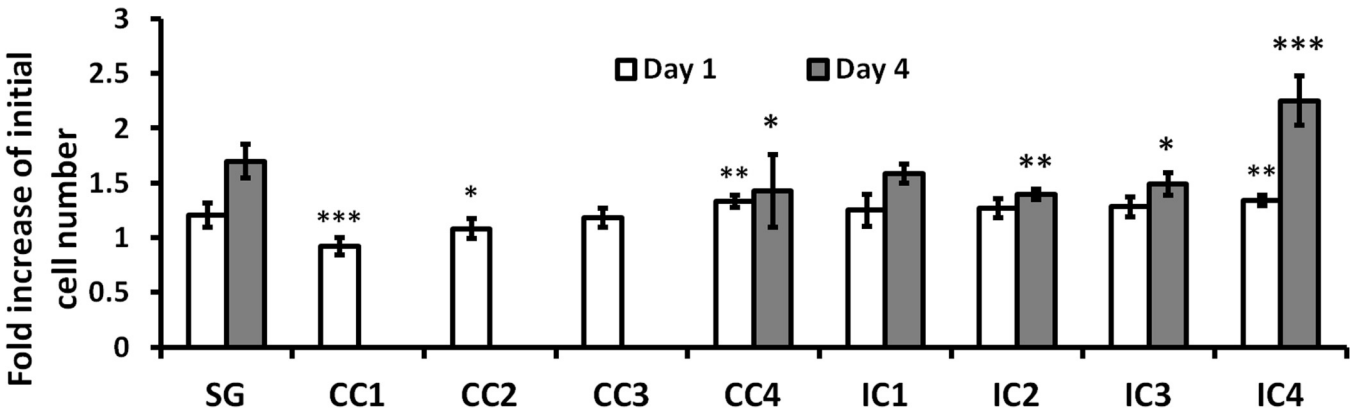

FIG. 8. Cell number increment after 4 days of flow in different experimental groups. SG-static culture on modified glass. CC1 to CC4—continuous flow chamber 1 to 4. IC1 to IC4—intermittent flow chamber 1 to 4. *$p < 0.05$, **$p < 0.01$, and ***$p < 0.001$.

TABLE I. List of primers for RT-PCR.

Beta actin forward	AGGCCAACCGTGAAAAGATG	107 bp
Beta actin reverse	GGTACGACCAGAGGCATACA	
ALP forward	AACGTCAATTAACGGCTGACAC	139 bp
ALP reverse	CACAAATGAGTTGGTAAGGCAGG	
MMP13 forward	GTGACTCTTGCGGGAATCCT	151 bp
MMP13 reverse	CAGGCACTCCACATCTTGGT	
Runx2 forward	TAGCGGCAGAATGGATGAGT	172 bp
Runx2 reverse	CACAACTGGGGAGTGAATGAGA	

F. Real time-polymerase chain reaction (RT-PCR) and ALP activity

Cells were extracted from the chambers after 1 day and 4 days, and RT-PCR was performed for three genes of interest, namely, ALP, runx2, and matrix metallopeptidase 13 (mmp13). Beta-actin (β-act) was selected as the reference gene. The primers for these genes are listed in Table I. After 1 day of flow, we could observe an increase in the expression level of these genes in the intermittent experimental group than the control (Fig. 9). However, the fold induction levels were similar or less than the control in first three chambers of the continuous flow group. We believe that the reduced expression levels of these genes are a result of shear injury in these chambers. The reduction was significant for all genes in CC1, two genes (mmp13 and runx2) in CC2, and only one gene (mmp13) in CC3. However, in CC4, there was upregulation in expression for all genes. The ALP mRNA expression was significantly high in IC1, IC3, and IC4. IC1 also had significant increase in fold induction of mmp13 and runx2. ALP activity was significantly elevated in all continuous flow chambers. In intermittent flow chambers, it was either similar to the control (IC3, IC4) or significantly low (IC1, IC2). mRNA expression regulation after mechanical loading can be detected earlier than protein level expression.[38] As we performed RT-PCR and ALP activity assays right after a flow phase, we believe that there was not enough time for replication of gene expression at the protein level for ALP. Hence, there is a difference in their magnitude in intermittent flow groups.

After 4 days of flow, cells detached from the first three chambers of the continuous flow group. Hence, gene expression studies and ALP activity assay could not be performed for them. At day 4, CC4 was showing higher ALP activity, but none of the genes showed significant increase in gene expression (Fig. 10). However, all intermittent experiments were showing an increase in gene expression at day 4 with statistical significance. It was witnessed that IC3, where shear stress is 10 mPa, has the highest fold change in gene expression levels with statistical significance for all the above-mentioned genes (2.6, 3.2, and 2.9 for ALP, mmp13, and runx2, respectively). Similar increase was observed in its ALP activity too (2.7-fold). IC1 also had significant increase in mmp13 (6.1-fold) and runx2 (2.9-fold) expression. Nonetheless, this increase was detected neither in ALP gene expression nor in its

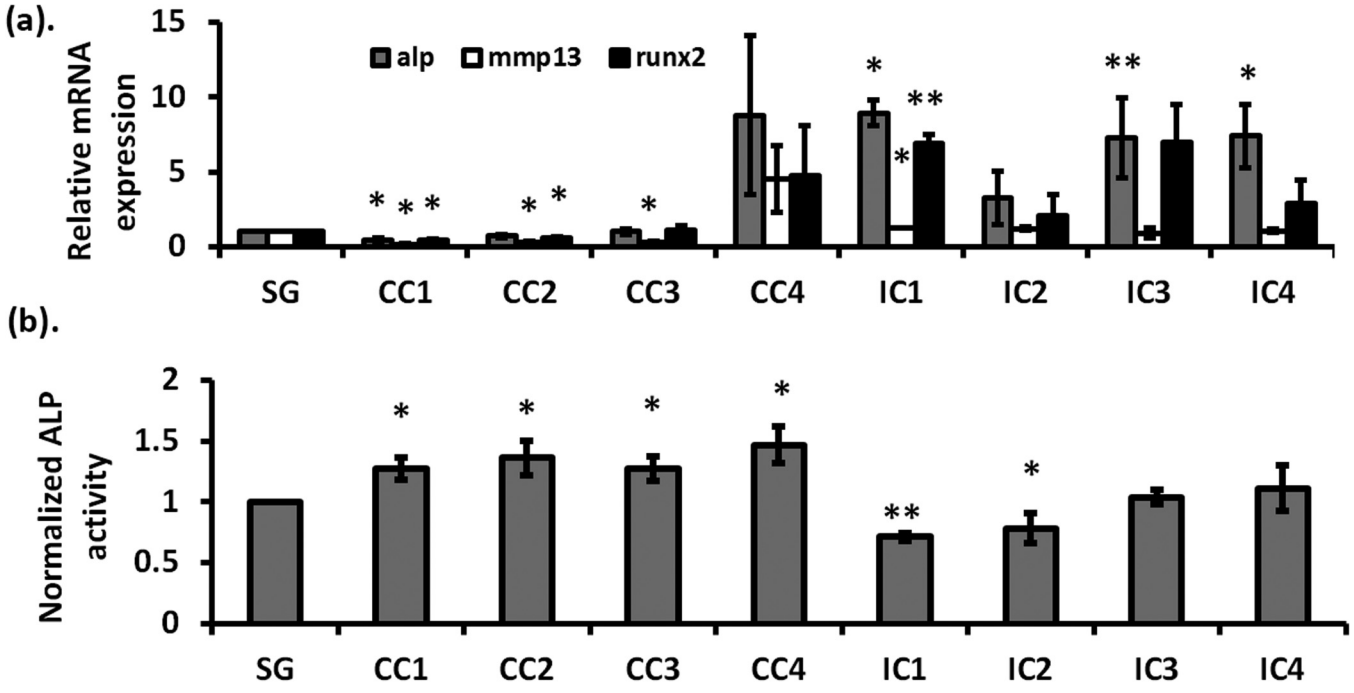

FIG. 9. (a) Gene expression profile and (b) ALP activity in different experimental groups after 1 day of flow. CC1 to CC4—continuous flow chamber 1 to 4. IC1 to IC4—intermittent flow chamber 1 to 4. SG-static culture on modified glass, SP-static culture on plastic. *$p < 0.05$, **$p < 0.01$, and ***$p < 0.001$.

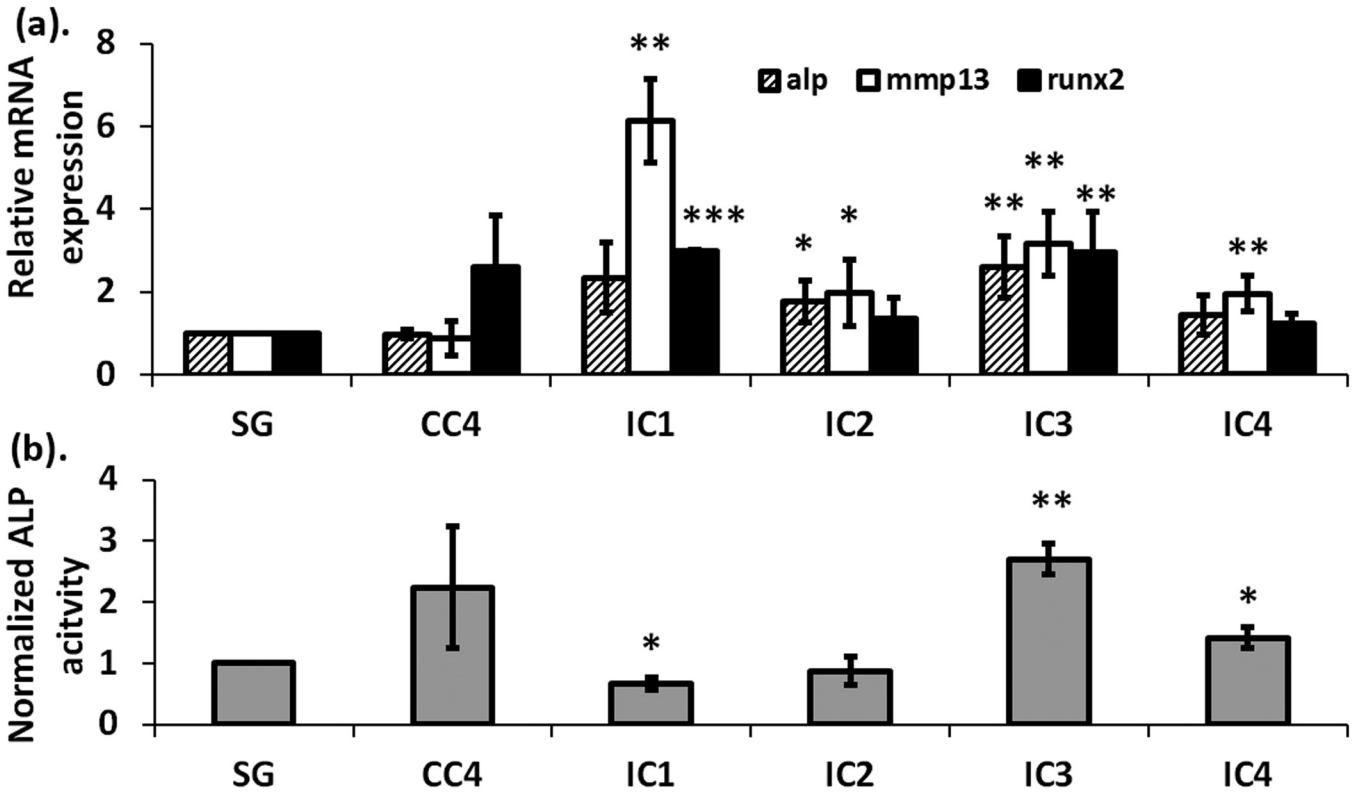

FIG. 10. (a) Gene expression profile and (b) ALP activity in different experimental groups after 4 days of flow. SG-static culture on modified glass, CC1 to CC4—continuous flow chamber 1 to 4. IC1 to IC4—intermittent flow chamber 1 to 4. *$p < 0.05$, **$p < 0.01$, and ***$p < 0.001$.

activity. Rather, the ALP activity of this group was significantly less than the control after 4 days, which failed to provide conclusive evidence for its suitability in osteogenic differentiation.

IV. DISCUSSION

Electrical analogy of hydraulic resistance can be applied to microfluidic networks to determine the flow parameters in them. When there are multiple channels required in a device, it becomes cumbersome to design them due to the increase in the number of variables. Optimization techniques help in such conditions to effectively design the channels and generate a highly efficient device.[39] With this idea, we carried out minimization of our objective function that is the summation of all fluidic resistances in the device. This led to the design of the logarithmic shear stress profile ranging four orders of magnitude. An important aspect of the device is that in all culture chambers, cells experience similar conditions except for FSS. As the device has four separate outlets, validation of the flow rate distribution could be done just by measuring the volume collected. Each culture chamber had individual seeding inlets for cells too. As per the design, removal and seeding of cells from a chamber through these inlets with a closed device inlet do not disturb the cells in other chambers. Thus, our device provides a better platform for both on-chip and off-chip analyses. Also, the total channel length is least possible, which enabled us to use the device for long runs without the issue of clogging. We also improved ECM (collagen) adsorption to cell culture surface by precoating it with APTES.[34] This enabled our device to provide a better cell culture surface.

Along with chemical signals, mechanical signals also influence cell behavior and function significantly. Mechanical forces help in tissue development and growth. Moreover, they play a vital role in many diseased conditions.[40,41] Study of a signal like FSS is very crucial, as cells are continually exposed to it in various tissues. FSS control of MSC fate can give new directions to bone tissue engineering. Steady 2D flow has been shown to induce cell cycle arrest in MSCs, whereas the oscillatory flow tends to increase cell proliferation.[42] Furthermore, dose-dependent reduction in MSC proliferation was reported earlier in steady flow with most cells arrested in the G0 or G1 phase.[37] High FSS has been known to impact cell morphology, cell–cell interaction, and matrix production. However, lower stresses have been found to increase cell proliferation and viability in a 3D perfusion system as well.[15]

Mmp13 was a gene of interest in our study, which encodes collagenase 3, an enzyme required for bone matrix mineralization. It is not only a marker of osteogenic differentiation, but it has also

been found as an essential link between the mechanical signal and MSC behavior. In response to tensile loading, earlier literature shows higher protein level expression of mmp13 but no change in mRNA level.[43] Though increment of this gene at the mRNA level was not evident after the first day, it was witnessed after 4 days of fluid flow in our study. This demonstrates that FSS might act differently on MSCs compared to other mechanical signals like tension. ALP is essential in mineralization of bone tissue via its enzymatic hydrolysis activity. Upregulation of ALP and runx2 gene is recognized as early markers of osteogenic differentiation.[13] Such upregulation was observed in all intermittent flow groups at all the time points. However, the expression levels were not found to be dose dependent in our observations. After 1 day of flow, the gene expression values were downregulated in the continuous flow group except CC4. Nonetheless, significant ALP activity was observed in all of them that show initial upregulation of ALP activity at high continuous shear. This upregulation also did not have any dose dependency effect. After 4 days, ALP activity was higher at low FSS in intermittent as well as in continuous groups. Similar magnitude of shear has been shown to induce osteogenesis in earlier works too.[11] Gene expression levels of all genes in IC1 and IC3 were higher than IC2 and IC4 at day 4. In IC1, though gene expression levels were higher, it was not correlating with ALP activity. This indicates that mechanotransduction pathways act differently at different shear levels for these genes. After 4 days, all gene expressions and ALP activity of IC3 were found to be higher compared to other groups, which show osteogenic differentiation of rBMSCs is superior in this range of intermittent FSS, i.e., 10 mPa. The shear stress experienced in human bone marrow is roughly between 0.037 and 0.14 Pa.[31] Osteoblast cells also experience interstitial-like flow.[44] We believe shear magnitudes in marrow will be even lesser in rats due to their smaller body size which might be the reason rBMSCs favor 10 mPa shear range for osteogenic differentiation.

Markers of mechanotransduction like Ca^{2+} movement, ERK phosphorylation, etc., have been found to be higher in the pulsatile flow than steady. Or, the impulse of the mechanical signal acts better than continuous signals.[45] Bone derived cells also become adaptive to mechanical stimulation if they are constantly subjected to this stimulation for a long time. Insertion of rest between loading can enhance osteogenesis effectively.[13] This effect was confirmed in intermittent experimental groups with better osteogenic differentiation. We did not observe any replication of trend neither in gene expression nor in ALP activity at both the time points. This suggests that the early osteogenesis response and late osteogenesis response may be different with the FSS signal.

We observed cell detachment in chambers 1, 2, and 3 in continuous shear flow experiments. It has been reported that mammalian cells like Chinese hamster ovaries (CHO) and human embryonic kidney (HEK) cells showed necrotic cell death when subjected to hydrodynamic shear stress of 1 Pa in simple shear flow.[46] Shear stress of 2.5 mPa has been shown to induce vacuolated structures after only 3 h of flow in intestinal epithelial cells. The molecular mechanism behind this vacuole formation has been found to involve central components of the autophagy pathway (through autophagy related 5 and microtubule-associated proteins 1A/1B light chain 3B genes).[47] High FSS has also shown to induce injury in rBMSCs. Washing off and twisting of rBMSCs have been observed after only 1 day of culture in previous studies.[48] It also shows reduced expression of growth factors like transforming growth factor beta (TGF-β), basic fibroblast growth factor (bFGF), vascular endothelial growth factor (VEGF), and platelet-derived growth factor (PDGF) in continuous flow conditions.[49] Evidence of similar reduced gene expression was observed in ALP, mmp13, and runx2 after 1 day in CC1, CC2, and CC3 in the present study. After 4 days of continuous flow, cell detachment or clump formation was observed even at 10 mPa of FSS. This behavior was accompanied with vacuole-like structures formation inside cells (Fig. S5 in the supplementary material). As reported earlier, mouse MSCs were viable and proliferating after 12 days of flow at shear of 1 mPa to 1 μPa.[50] However, as of our knowledge, none of the earlier literature studies show long-term behavior of rBMSCs on high to moderate FSS ($\geq$10 mPa) that could explain such detachment. We hypothesize that this might be because of non-exposure of rBMSCs to continuous shear in their native environment.

V. CONCLUSION

Microfluidic devices developed in recent times can produce shear stresses of very small range in one run. In order to cover a broad range, either the device has to be changed or two or more devices have to be operated in parallel. In this study, we present the design of a microfluidic shear device, which has the capability to generate fluid shear of four different orders in the physiologic range. The system employs an analogous resistance model for flow distribution, which was confirmed by outflow measurements. Hydraulic resistances were optimized to make the device compact. The 3D numerical simulation used helped in finding shear stresses corresponding to different operating flow rates for the final setup. Usage of very small volume of sample in the device can facilitate the study of rare and expensive samples. Our device will support any adherent cell type on which FSS effects can be studied. Applicability of the stated optimization method can be extended to design various microfluidic flow distribution scenarios.

Finally, the behavior of rat bone marrow mesenchymal stem cells was examined in the microfluidic device. Strong dependence of cell proliferation and differentiation characteristic was observed with the magnitude and way of application of shear stress. We found upregulation of both differentiation and proliferation in low intermittent flow experiments but at different magnitudes of stresses. Interestingly, cell detachment in the continuous flow group was seen after 4 days even at medium shear. The reason for this is still unclear, and further studies are needed to reveal such behavior of rBMSCs.

SUPPLEMENTARY MATERIAL

See the supplementary material for device image, FACS data, day wise morphology of cells, ALP activity without chemical stimulus, simulation data, and Video 1 and Video 2 for visualization of the logarithmic flow distribution in the device.

ACKNOWLEDGMENTS

The authors thank Professor Amitava Das Gupta and Professor Nandita Das Gupta of MEMS Laboratory, Department of Electrical Engineering, IIT Madras for the photolithography facility for the fabrication of the microfluidic device. There are no conflicts of interest to declare.

DATA AVAILABILITY

The data that support the findings of this study are available within the article and its supplementary material.

REFERENCES

[1]J. Ando and K. Yamamoto, Circ. J. **73**, 1983 (2009).
[2]J. Shemesh, I. Jalilian, A. Shi, G. Heng Yeoh, M. L. Knothe Tate, and M. Ebrahimi Warkiani, Lab Chip **15**, 4114 (2015).
[3]K. J. Jeon, S. H. Park, J. W. Shin, Y. G. Kang, J.-S. Hyun, M. J. Oh, S. Y. Kim, and J.-W. Shin, J. Biosci. Bioeng. **117**, 242 (2014).
[4]Y. Huang, X. Jia, K. Bai, X. Gong, and Y. Fan, Arch. Med. Res. **41**, 497 (2010).
[5]M. J. Song, S. M. Brady-Kalnay, S. H. McBride, P. Phillips-Mason, D. Dean, and M. L. K. Tate, PLoS One **7**, e43601 (2012).
[6]Y. J. Li, N. N. Batra, L. You, S. C. Meier, I. a Coe, C. E. Yellowley, and C. R. Jacobs, J. Orthop. Res. **22**, 1283 (2004).
[7]E. Stavenschi, M. N. Labour, and D. A. Hoey, J. Biomech. **55**, 99 (2017).
[8]D. Yue, M. Zhang, J. Lu, J. Zhou, Y. Bai, and J. Pan, J. Cell. Physiol. **234**, 16312 (2019).
[9]Y. C. Kuo, T. H. Chang, W. T. Hsu, J. Zhou, H. H. Lee, J. Hui-Chun Ho, S. Chien, and O. Kuang-Sheng, Stem Cells **33**, 429 (2015).
[10]R. C. Riddle, A. F. Taylor, D. C. Genetos, and H. J. Donahue, Am. J. Physiol. Cell Physiol. **290**, C776 (2006).
[11]K. M. Kim, Y. J. Choi, J. H. Hwang, A. R. Kim, H. J. Cho, E. S. Hwang, J. Y. Park, S. H. Lee, and J. H. Hong, PLoS One **9**, e92427 (2014).
[12]W. Yu, H. Qu, G. Hu, Q. Zhang, K. Song, H. Guan, T. Liu, and J. Qin, PLoS One **9**, e89966 (2014).
[13]L. Liu, B. Yu, J. Chen, Z. Tang, C. Zong, D. Shen, Q. Zheng, X. Tong, C. Gao, and J. Wang, Biomech. Model. Mechanobiol. **11**, 391 (2012).
[14]C. F. Dewey, S. R. Bussolari, M. A. Gimbrone, and P. F. Davies, J. Biomech. Eng. **103**, 177 (1981).
[15]F. Zhao, R. Chella, and T. Ma, Biotechnol. Bioeng. **96**, 584 (2007).
[16]G. Yourek, S. M. McCormick, J. J. Mao, and G. C. Reilly, Regen. Med. **5**, 713 (2010).
[17]L. C. Delon, Z. Guo, A. Oszmiana, C. C. Chien, R. Gibson, C. Prestidge, and B. Thierry, Biomaterials **225**, 119521 (2019).
[18]L. Chau, M. Doran, and J. Cooper-White, Lab Chip **9**, 1897 (2009).
[19]R. Booth, S. Noh, and H. Kim, Lab Chip **14**, 1880 (2014).
[20]S. Kou, L. Pan, D. van Noort, G. Meng, X. Wu, H. Sun, J. Xu, and I. Lee, Biochem. Biophys. Res. Commun. **408**, 350 (2011).
[21]W. Zhong, H. Ma, S. Wang, X. Gao, W. Zhang, and J. Qin, Microfluid. Nanofluid. **15**, 763 (2013).
[22]J. M. Rutkowski and M. A. Swartz, Trends Cell Biol. **17**, 44 (2007).
[23]D. P. Gaver and S. M. Kute, Biophys. J. **75**, 721 (1998).
[24]N. Murugesan, P. Dhar, T. Panda, and S. K. Das, Biomicrofluidics **11**, 024108 (2017).
[25]M. Soleimani and S. Nadri, Nat. Protoc. **4**, 102 (2009).
[26]P. Vidyasekar, P. Shyamsunder, S. K. Sahoo, and R. S. Verma, Vitr. Cell. Dev. Biol. Anim. **52**, 204 (2016).
[27]P. Sreejit and R. S. Verma, Cell Tissue Res. **353**, 443 (2013).
[28]R. Santhakumar, P. Vidyasekar, and R. S. Verma, PLoS One **9**, 1 (2014).
[29]S. K. Dash, R. S. Verma, and S. K. Das, in *Proceedings of the Annual International Conference of the IEEE Engineering in Medicine and Biology Society, 2015 November* (IEEE, 2015), p. 3209.
[30]H. Bruus, *Theoretical Microfluidics* (OUP, Oxford, 2007).
[31]G. Follain, D. Herrmann, S. Harlepp, V. Hyenne, N. Osmani, S. C. Warren, P. Timpson, and J. G. Goetz, Nat. Rev. Cancer **20**, 107 (2020).
[32]T. Gervais, J. El-Ali, A. Günther, and K. F. Jensen, Lab Chip **6**, 500 (2006).
[33]I. D. Johnston, D. K. McCluskey, C. K. L. Tan, and M. C. Tracey, J. Micromech. Microeng. **24**, 035017 (2014).
[34]M. Nobles and N. J. Abbott, Endothel. J. Endothel. Cell Res. **4**, 297 (1996).
[35]J. M. Curran, R. Chen, and J. A. Hunt, Biomaterials **26**, 7057 (2005).
[36]M. Maleki, F. Ghanbarvand, M. R. Behvarz, M. Ejtemaei, and E. Ghadirkhomi, Int. J. Stem Cells **7**, 118 (2014).
[37]L. Zhao, C. Fan, Y. Zhang, Y. Yang, D. Wang, C. Deng, W. Hu, Z. Ma, S. Jiang, S. Di, Z. Qin, J. Lv, Y. Sun, and W. Yi, Sci. Rep. **6**, 1 (2016).
[38]A. I. Barakat and D. K. Lieu, Cell Biochem. Biophys. **38**, 323 (2003).
[39]N. Hamadneh, W. Khan, and S. Tilahun, Machines **6**, 26 (2018).
[40]N. Baeyens, C. Bandyopadhyay, B. G. Coon, S. Yun, and M. A. Schwartz, J. Clin. Invest. **126**, 821 (2016).
[41]M. L. Knothe Tate, J. Biomech. **36**, 1409 (2003).
[42]B. D. Riehl, H. J. Donahue, and J. Y. Lim, *Fluid Flow Control of Stem Cells With Investigation of Mechanotransduction Pathways* (Elsevier Inc., 2017).
[43]G. Kasper, J. D. Glaeser, S. Geissler, A. Ode, J. Tuischer, G. Matziolis, C. Perka, and G. N. Duda, Stem Cells **25**, 1985 (2007).
[44]C. Wittkowske, G. C. Reilly, D. Lacroix, and C. M. Perrault, Front. Bioeng. Biotechnol. **4**, 87 (2016).
[45]M. R. Kreke, L. A. Sharp, Y. Woo Lee, and A. S. Goldstein, Tissue Eng. Part A **14**, 529 (2008).
[46]T. Tanzeglock, M. Soos, G. Stephanopoulos, and M. Morbidelli, Biotechnol. Bioeng. **104**, 360 (2009).
[47]S. W. Kim, J. Ehrman, M. R. Ahn, J. Kondo, A. A. M. Lopez, Y. S. Oh, X. H. Kim, S. W. Crawley, J. R. Goldenring, M. J. Tyska, E. C. Rericha, and K. S. Lau, Mol. Biol. Cell **28**, 3043 (2017).
[48]K. Bai, Y. Huang, X. Jia, Y. Fan, and W. Wang, J. Biomech. **43**, 1176 (2010).
[49]Y. Yang, C. Fan, C. Deng, L. Zhao, W. Hu, S. Di, Z. Ma, Y. Zhang, Z. Qin, Z. Jin, X. Yan, S. Jiang, Y. Sun, and W. Yi, J. Pineal Res. **60**, 228 (2016).
[50]X. Gao, X. Zhang, H. Xu, B. Zhou, W. Wen, and J. Qin, Biomicrofluidics **8**, 052008 (2014).